



Cite this: *Green Chem.*, 2025, **27**, 5063

Received 12th December 2024,  
Accepted 7th April 2025

DOI: 10.1039/d4gc06305h

[rsc.li/greenchem](https://rsc.li/greenchem)

# Efficient continuous flow oxidation of furfural to maleic anhydride using O<sub>2</sub> as a green oxidant†

Jonas Mortier,  Christian V. Stevens  and Thomas S. A. Heugebaert  \*

This research investigates different oxidative pathways to obtain maleic anhydride starting from the biorenewable furfural in continuous flow. A single step O<sub>2</sub><sup>1</sup> oxidation towards maleic anhydride was investigated but found to lack selectivity. Nonetheless, the resulting product analysis provided valuable insight into the possible reaction mechanism, uncovering an interesting solvent effect. Building on this, an existing slow reacting two-step pathway was translated towards a continuous one, achieving a fast and highly productive conversion towards maleic anhydride while aligning with green chemistry principles.

## Green foundation

1. In this work, *n*-butane and/or benzene were replaced with biorenewable furfural as feedstock for maleic anhydride. Previous such valorization pathways suffer from low productivity and selectivity. We have identified the underlying mechanistic origins of the selectivity issue, which inherently dictates a two-step catalytic approach.
2. By leveraging continuous flow chemistry a more efficient and competitive process was developed with high selectivity (98%), and facile scalability. We significantly reduced catalyst loadings (2%) compared to the existing batch process (5 & 10%) and replaced acetonitrile with ethyl acetate in the second reaction step; while also drastically reducing reaction time (30 min vs. 480 min).
3. Future research should prioritize exploring the use of heterogeneous, easily removed and recycled catalysts, such as polymer-immobilized TEMPO (PIPO). However, this topic falls outside the scope of the present study.

## Introduction

The global chemical industry, traditionally reliant on petrochemical processes, faces increasing pressure to transition to more sustainable practices due to environmental concerns and the finite nature of fossil resources. This shift is critical not only for reducing greenhouse gas emissions but also for minimizing the environmental footprint of chemical production.<sup>1</sup> A promising approach to achieving this goal is through the principles of green chemistry, which emphasize the design of chemical products and processes that reduce or eliminate the use and generation of hazardous substances. Key principles of green chemistry include the use of renewable feedstocks, energy efficiency, and waste minimization. By adhering to these principles, the industry can move towards a more sustainable, bio-based economy.<sup>2</sup>

Furfural (FUR), a valuable platform chemical derived from lignocellulosic biomass, has emerged as a key renewable feed-

stock with the potential to replace petrochemical precursors in various industrial processes.<sup>3</sup> Lignocellulosic biomass, which includes agricultural residues and non-food crops, offers a renewable and abundant source of carbon. FUR is obtained *via* the acid-catalyzed dehydration of pentoses present in hemicellulose and serves as an intermediate for the synthesis of numerous chemicals.<sup>4</sup> One particularly valuable transformation of FUR is its conversion to maleic anhydride (MA), a versatile chemical used in the production of resins, plastics, and agrochemicals.<sup>5,6</sup> Traditionally, MA is produced from benzene or *n*-butane through an energy-intensive process employing a phosphorus vanadium oxide catalyst at high temperatures (Fig. 1).<sup>7–10</sup>

Thus, developing a green and efficient method to convert FUR to MA is highly desirable. In recent years, various one-step oxidations producing MA directly from FUR have been explored. Among these methods, the vanadium-catalyzed aerobic oxidation of furfural has been the most widely studied. Using the same catalysts as the traditional petroleum-based process, medium to high yields are only obtained after exposing gas-phase furfural to temperatures of 300–340 °C.<sup>11–14</sup> Besides the low productivity and the risk of overoxidation, catalyst deactivation at these temperatures also poses a major problem. These problems could be minimized by performing

Department of Green Chemistry and Technology, Faculty of Bioscience Engineering, Ghent University, Coupure Links 653, 9000 Ghent, Belgium.

E-mail: [Thomas.Heugebaert@UGent.be](mailto:Thomas.Heugebaert@UGent.be)

† Electronic supplementary information (ESI) available. See DOI: <https://doi.org/10.1039/d4gc06305h>



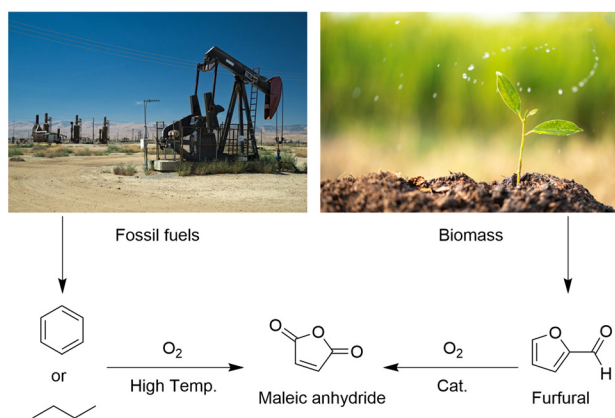


**Fig. 1** A comparison between the traditional synthesis of maleic anhydride starting from benzene or *n*-butane and the biorenewable route starting from furfural.

the oxidations in solution-phase at lower temperature, but long reaction times, low selectivity and the hydrolysis of MA to maleic acid make this approach non-optimal as well (Table S1, ESI†).<sup>15–17</sup>

While maleic acid remains valuable—since it can be isomerized into fumaric acid,<sup>18,19</sup> a key precursor for bio-based polyesters<sup>20,21</sup>—maleic anhydride is generally preferred as a building block due to its higher reactivity, particularly in Diels–Alder-type reactions<sup>22–24</sup> and photochemical [2 + 2] cycloadditions.<sup>25,26</sup> Moreover, maleic anhydride can readily hydrolyze in water under mild conditions,<sup>27</sup> whereas reversing this process typically requires high temperatures and additional catalysts and additives,<sup>28–30</sup> making it the more reactive and energetically enriched form of maleic acid.

A more convenient method to oxidize furfural has been examined by Zhang *et al.*<sup>31</sup> where a solution of formic acid/H<sub>2</sub>O<sub>2</sub> and furfural is heated at 60 °C to achieve 95% conversion after 4 hours of reaction time. However, due to the choice of solvent, complete hydrolysis occurred resulting in the formation of the ring-opened maleic acid as final product. It should also be noted that in this reaction, oxygen has been replaced by the less desired hydrogen peroxide as oxidant.

To step away from high temperatures and protic solvents that might catalyze the hydrolysis of MA, two direct photocatalytic aerobic oxidations were examined (Table 1). In both methods, the authors reason that the photocatalyst generates multiple reactive oxygen species, which subsequently lead to the oxidation of furfural. Although these reactions can be operated at room temperature, the reactive oxygen species give rise to many byproducts with 5-hydroxy-2(5*H*)-furanone 3 (HFO) being the most prominent one. The low selectivity and long reaction time currently make this method unsuitable for industrial-scale applications.

Intrigued by these results showing the simultaneous formation of HFO 3 and MA 2, our aim was to determine the cause of this unusual outcome and explore whether continuous flow intensification strategies could enhance the reaction

**Table 1** Singlet oxygen oxidation of furfural to maleic anhydride via different catalysts

Ref.	Solvent	Cat.	2/3 (%)
32	MeCN/DCM (5/1)	CuO <sub>x</sub> /Nb <sub>2</sub> O <sub>5</sub>	37/22 (24 h) <sup>a</sup>
33	MeCN	Mesoporous C <sub>3</sub> N <sub>4</sub>	42/33 (30 h) <sup>b</sup>

<sup>a</sup> Yield of corresponding products is displayed. <sup>b</sup> Selectivity of corresponding products is displayed.

selectivity. Upon reviewing these two previous photocatalytic methods, several key similarities emerge. In both approaches, the final products consist of a mixture of MA 2 and HFO 3, with similar ratios (1.7 vs. 1.3). Moreover, singlet oxygen (O<sub>2</sub><sup>1</sup>) was identified as the primary reactive oxygen species driving the reactions. Both studies also suggested that superoxide radicals (O<sub>2</sub><sup>•−</sup>) play a role, although when superoxide radical quencher benzoquinone (BQ) was introduced, the reaction only experienced a slight decrease in conversion, rather than ceasing entirely. This evidence suggests that singlet oxygen may be the sole active species. However, if singlet oxygen were the only reactive species, previous literature indicates that furfural should fully convert to HFO under similar conditions.<sup>27,34–37</sup> It is worth noting that in previously cited literature, the conversion of FUR to HFO was consistently carried out in protic, nucleophilic solvents such as EtOH, MeOH, or H<sub>2</sub>O. These mildly nucleophilic solvents help resolve the intermediate endoperoxide through nucleophilic attack on the aldehyde moiety, leading to the formation of HFO 3 (Fig. 2). In contrast, when non-nucleophilic solvents like MeCN or DCM are used, the inability to efficiently resolve the endoperoxide intermediate may result in the production of various other products, such as MA 2.

## Results and discussion

### One-step continuous flow O<sub>2</sub><sup>1</sup> oxidation of FUR towards various reaction products

To test the hypothesis that singlet oxygen oxidation of furfural in a non-nucleophilic solvent like acetonitrile leads to a combination of MA and HFO, methylene blue was used as photosensitizer to generate singlet oxygen. To overcome the attenuation effect which limits the efficient penetration of light throughout the reaction mixture, a continuous flow reactor is used. The reaction rate was remarkably high, achieving almost full conversion after only 6.5 minutes. Interestingly, a very similar 2/3 ratio of around 1.3 was achieved, thus confirming their inherent co-production under singlet oxygen mediated oxidation (Table 2, entries 1–3). When initially conducting the reaction however, we observed variability in the 2/3 ratio across duplicate experiments, along with a poor mass balance. We



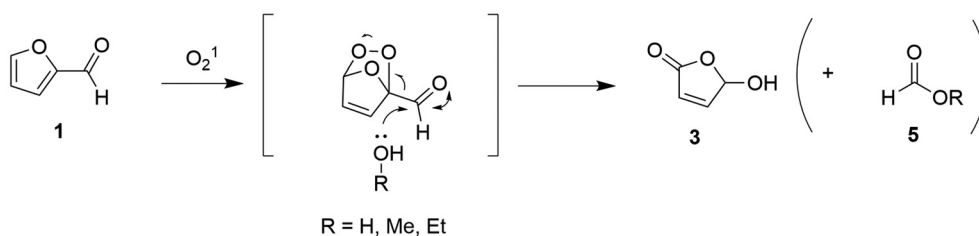


Fig. 2 Mechanistic pathway for the oxidation of furfural **1** towards HFO **3** in solvent ROH (R = H, Me, Et).

Table 2 Singlet oxygen oxidation of FUR **1** towards various products

Entry	Solvent	Pump flow rate (ml min <sup>-1</sup> )	O <sub>2</sub> flow rate (ml <sub>N</sub> min <sup>-1</sup> )	Residence time <sup>a</sup> (min)	Conv. <b>1</b> <sup>b</sup> (%)	Yield <sup>c</sup> <b>2/3/6/7/8</b> (%)
1	MeCN	0.3	10	45	100	29/23/20/4/7 <sup>d</sup>
2	MeCN	1.5	20	6.5	98	27/21/19/2/5 <sup>d</sup>
3	MeCN	3	40	3.5	86	25/19/18/2/4 <sup>d</sup>
4	Dry MeCN	3	40	3.5	87	24/19/19/2/5 <sup>d</sup>
5	MeCN/H <sub>2</sub> O (24/1)	3	40	3.5	96	23/44/9/1/3
6	MeCN/H <sub>2</sub> O (14/1)	3	40	3.5	93	17/54/1/1/3
7	MeCN/H <sub>2</sub> O (9/1)	3	40	3.5	96	13/63/0/0/2
8	MeCN/H <sub>2</sub> O (4/1)	3	40	3.5	95	2/89/0/0/0
9	MeCN/H <sub>2</sub> O (1/1)	3	40	3.5	81	0/77/0/0/0

<sup>a</sup> Residence time determined experimentally. <sup>b</sup> Conversion determined *via* quantitative HPLC analysis. <sup>c</sup> Yield determined *via* quantitative <sup>1</sup>H-NMR analysis with mesitylene as internal standard, unless stated otherwise. <sup>d</sup> Yield determined *via* quantitative GC-MS analysis (**2**) and quantitative <sup>1</sup>H-NMR analysis (**3**, **6**, **7** and **8**).

later determined that maleic anhydride **2** had sublimated during the evaporatory work-up process. To prevent this issue, we opted to directly analyze the reaction mixture using <sup>1</sup>H-NMR without performing solvent evaporation. This approach revealed several additional signals that had gone undetected in previous literature reports. The volatility and/or fragility of these side products made it challenging to fully characterize all of them. However, *cis*-β-formylacrylic acid (CBF) **6** was identified as the major side product. *trans*-β-Formylacrylic acid (TBF) **7** was also formed in smaller quantities along with, interestingly, the 5-(formyloxy)-2(5H)-furanone (FOF) **8** and formic acid. The formation of CBF **6** was also reported in the work of Kailasam *et al.*,<sup>33</sup> and is a known tautomeric product of HFO **3**.<sup>38</sup> As the MeCN/H<sub>2</sub>O solvent mixture shifts more towards H<sub>2</sub>O, it is seen that HFO emerges as the sole product (Table 2, entries 5–9). This emphasizes the critical importance of solvent effects on product formation, as increasing the water content directs the oxidation to proceed *via* the well-known nucleophilic solvent induced pathway delivering formic acid and HFO

(Fig. 2). As more water is added to the reaction medium, the nucleophilic attack pathway will become the more dominant one resulting in more HFO **3** formation. This trend continues until a 1 : 1 H<sub>2</sub>O/MeCN ratio is reached, where HFO **3** becomes the sole product (Table 2, entry 9).

In the absence of water though, the mechanism in which HFO and formic acid, but also MA are formed remains unclear. To rule out the possibility that HFO and formic acid formation in MeCN was caused by trace amounts of water present in the solvent, the experiment was repeated using strictly anhydrous MeCN, yielding the same result (Table 2, entry 4). Furthermore, when the reaction was conducted with 4% water intentionally added to the mixture, the HFO yield increased slightly but not dramatically (Table 2, entry 5). This observation confirms that trace amounts of water cannot fully account for the observed amounts of HFO and formic acid formation, and the classical nucleophilic mechanism (Fig. 2) is not the predominant one. A closer evaluation of the newly found side products however reveals that 5-(formyloxy)-2(5H)-



furanone **8** could be the result of a Baeyer–Villiger rearrangement, which has been proposed in several  $\text{H}_2\text{O}_2$ -mediated pathways towards maleic acid.<sup>31,39,40</sup> Interestingly, Yin and co-workers<sup>17</sup> observed the very closely related compound 5-acetoxy-2(5*H*)-furanone when performing a  $\text{H}_5\text{PV}_2\text{Mo}_{10}\text{O}_{40}$  catalyzed oxidation of furfural using acetic acid as solvent.

To evaluate whether **8**, or any of the other products might act as intermediates for MA formation, the reaction was carried out in batch and monitored over time. There is no indication that any of the products act as intermediates, as their yields increase throughout the reaction without any subsequent consumption (Fig. S14, ESI†). Similar results were observed in the continuous flow experiments, where nearly full

conversion was achieved within 6.5 minutes, and extending the reaction time to 45 minutes did not significantly alter the product ratios (Table 2, entries 1 and 2). Unfortunately, this indicates that, with this approach, the yield of maleic anhydride peaks at around 30%.

### Mechanism

A plausible mechanism to explain the formation of all reaction products begins with the generation of endoperoxide intermediate **9** via  $\text{O}_2^1$  oxidation (Fig. 3). In nucleophilic solvents, this endoperoxide would be resolved by a nucleophilic attack by the solvent resulting in HFO **3** formation (Fig. 2). When the reaction is performed in an anhydrous, non-nucleophilic

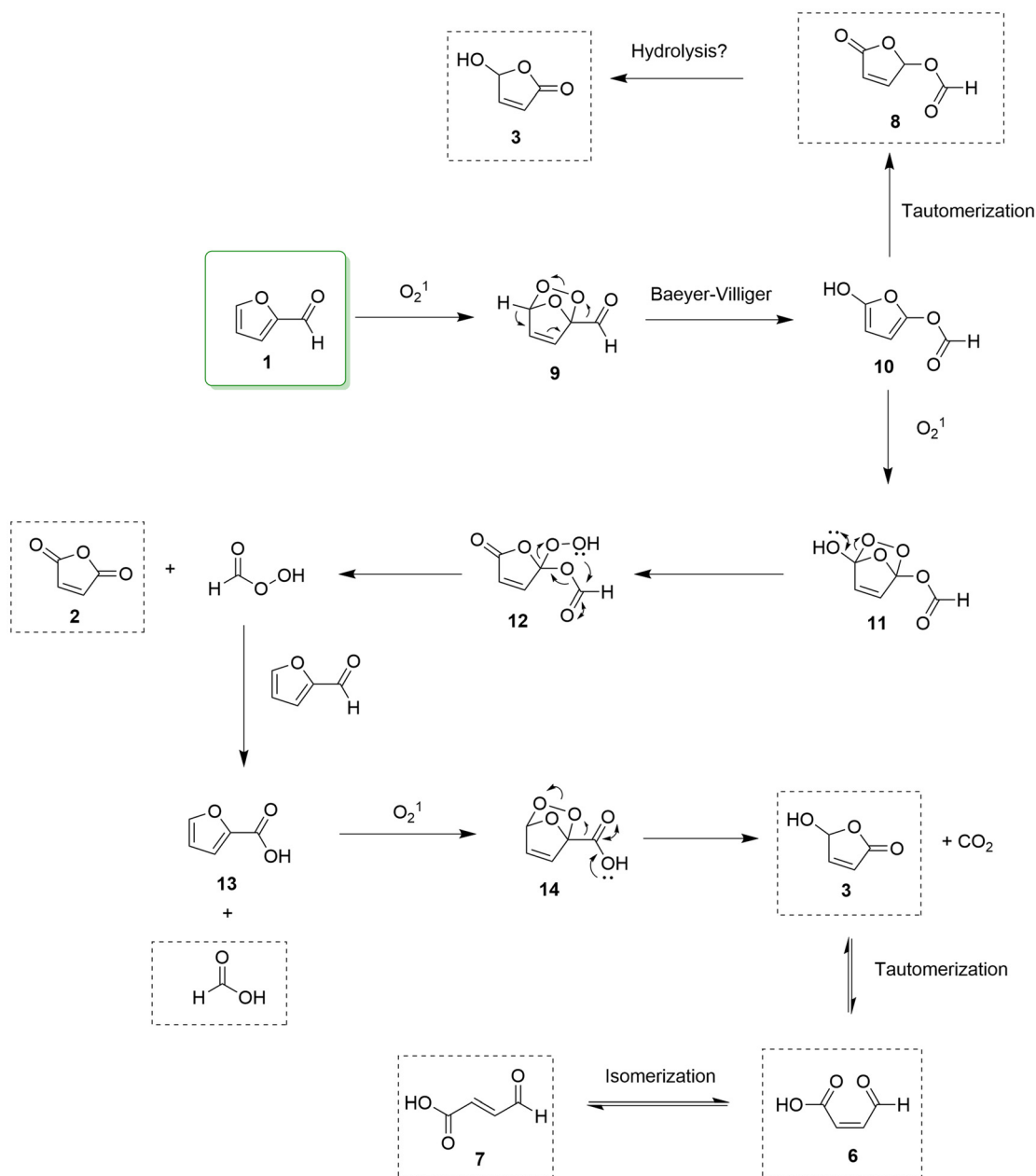


Fig. 3 Plausible pathway for the  $\text{O}_2^1$  oxidation of furfural towards various reaction products.



solvent like acetonitrile, it is proposed that a Baeyer-Villiger type of rearrangement will result in 5-hydroxy intermediate **10**. This intermediate can either tautomerize to its more stable keto-form **8** via a 1,4-rearrangement, which is detected in the reaction mixture, or alternatively will react with  $O_2$  to form a secondary endoperoxide intermediate **11**. The subsequent endoperoxide will open, resulting in hydroperoxide intermediate **12**, which rearranges into maleic anhydride **2** and performic acid. The performic acid formed in this step will then oxidize another molecule of furfural towards 2-furoic acid **13**, releasing formic acid as byproduct, as observed in the  $^1H$ -NMR spectrum. The resulting furoic acid will then react with  $O_2$ , followed by decarboxylation, to produce HFO **3** without requiring a nucleophilic solvent to resolve the endoperoxide **14**. HFO can then tautomerize into CBF **6**, which, in turn, can undergo *cis-trans* isomerization to form TBF **7**. In this way, for every molecule of maleic anhydride **2** formed, one molecule of performic acid would also be generated. This performic acid oxidizes furfural to produce one equivalent of 2-furoic acid **13**, which subsequently yields one equivalent of HFO **3**. HFO could then isomerize to form TBF **6** and CBF **7**. Based on this reasoning, the expected ratio of **2** to (**3** + **6** + **7**) in acetonitrile should be 1:1. However, in our experiments, the observed ratio is around 1:1.6 (Table 2, entries 1–4). While the hydrolysis of FOF **8** could explain the excess HFO, this is unlikely due to the very low water content. Instead, the surplus HFO and its isomers is attributed to a minor, as-yet-undiscovered pathway. Numerous studies suggest that 2-furoic acid **13** acts as a direct intermediate in furfural oxidation processes.<sup>31,33,40,41</sup> However, we did not detect this product in the  $^1H$ -NMR analysis of our reaction mixture. This absence could be explained if the subsequent reaction of 2-furoic acid with  $O_2$  to form HFO **3** occurs at a rate significantly faster—potentially an order of magnitude—than the overall reaction rate, making this intermediate undetectable during the reaction follow-up (Fig. S14, ESI†). Supporting this hypothesis, the reaction was conducted using 2-furoic acid **13** as the starting material, an exceptionally high reaction rate was observed, with nearly complete conversion to HFO **3** occurring within

just 20 seconds (Table 3). In the reaction mixture of this experiment, no formic acid was detected, consistent with the decarboxylation observed by Wang *et al.*, who reported a 1:1 ratio of HFO to  $CO_2$  during a  $CuO_x/Nb_2O_5$ -catalyzed furfural oxidation.<sup>32</sup> These experiments suggest that a parallel, direct oxidation of furfural to the intermediate 2-furoic acid **13** could account for the observed excess in HFO formation.

In conclusion, a one-step conversion of FUR to MA is subjected to various limitations. In literature it was seen that the need for high reaction temperatures in the gas phase vanadium-catalyzed oxidations gives rise to overoxidation resulting in lower yields, while solution-state reactions with the latter catalyst are plagued by long reaction times and only medium selectivity. The singlet oxygen oxidation of FUR to MA, on the other hand, proceeds at room temperature but exhibits low selectivity due to the inherent co-production of HFO.

### Two-step continuous flow oxidation of FUR towards MA

A more recent study by Feringa and co-workers<sup>27</sup> has suggested that a two-step pathway – first converting FUR to HFO, followed by the transformation of HFO to MA – may be more convenient. The photocatalytic conversion of FUR to HFO has been demonstrated in various studies and results in quantitative yield with short reaction times.<sup>27,36,37,42</sup> The bottleneck, however, is the TEMPO-mediated aerobic oxidation of HFO **3** to MA **2**, which takes 8 hours to complete resulting in a low productivity, in spite of the high catalyst loadings (Fig. 4).

By transitioning from a batch process to a continuous flow system, the key challenges of extended reaction times and high catalyst loadings can be effectively addressed, creating a truly

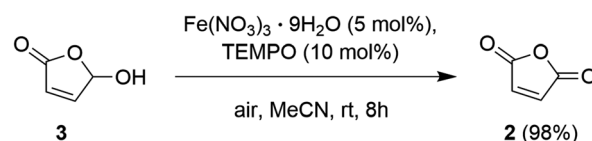
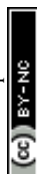


Fig. 4 TEMPO-mediated aerobic oxidation from HFO to MA (Feringa *et al.*, 2022).<sup>27</sup>

Table 3 Singlet oxygen oxidation of 2-furoic acid **13** towards HFO **3**

Entry <sup>a</sup>	Residence time <sup>b</sup>	Conv. <b>1</b> <sup>c</sup> (%)	Yield <b>3</b> <sup>c</sup> (%)
1	6.5 min	100	100
2	1.5 min	100	100
3	1 min	100	100
4	20 s	96	96

<sup>a</sup> All reactions were performed with a starting concentration of 0.2 M. <sup>b</sup> Residence time determined experimentally. <sup>c</sup> Conversion and yield determined *via* quantitative  $^1H$ -NMR analysis with mesitylene as internal standard.





efficient and productive pathway for converting FUR to MA. We will therefore focus on creating a straightforward, productive, and selective two-step synthesis in continuous flow, utilizing the TEMPO-mediated oxidation to convert the platform molecule FUR to MA previously described by Feringa and co-workers (Fig. 5).<sup>27</sup>

### Continuous flow O<sub>2</sub><sup>1</sup> of FUR to HFO

The continuous flow oxidation of furfural to HFO **3** by singlet oxygen has been well-documented in literature.<sup>36,37</sup> With methylene blue as the photosensitizer in MeOH, a residence time of 20 minutes was sufficient to achieve complete conversion with high selectivity (Table 4). From a sustainability standpoint, it is highly recommended to minimize purification steps between reaction steps while also paying attention to solvent recovery. In this instance, the only byproduct formed is methyl formate, which has a boiling point of 32 °C – significantly different from methanol, making it easier to separate during solvent recovery. This simplifies the purification process, lowering operational complexity and minimizing the environmental impact.

### Batch optimization of TEMPO-mediated oxidation of HFO to MA

The final step in the pathway consists of a TEMPO-catalyzed aerobic oxidation from HFO to MA. In 2011, Yu *et al.*<sup>43</sup> described a general method for the oxidation of alcohols to aldehydes/ketones, employing oxygen and catalytic amounts of TEMPO, Fe(NO<sub>3</sub>)<sub>3</sub> and table salt. In 2022, Feringa and co-workers<sup>27</sup> displayed how this method could convert HFO to MA quantitatively after 8 hours of stirring (Fig. 4). Before translating this reaction to continuous flow, the first optimization

reactions were carried out in batch starting with the reaction conditions that were already established for this method. Although it is preferable to choose a solvent that can be utilized in both reaction steps, adhering to the principle of reaction telescoping,<sup>44</sup> it was quickly realized that this would be impossible. A review of the literature reveals that all high-yielding singlet oxygen oxidations of FUR occur in protic solvents like MeOH, EtOH, H<sub>2</sub>O or a combination of prior solvents.<sup>27,34–37</sup> In contrast, for the aerobic oxidation of HFO **3** to MA **2**, even trace amounts of MeOH completely inhibited conversion, likely due to this method's tendency to oxidize MeOH itself (Table 5, entries 1 and 2). When performing the reaction in water on the other hand, <sup>1</sup>H-NMR analysis revealed that the desired conversion takes place, but maleic anhydride is immediately hydrolyzed to maleic acid (Table 5, entry 3). Furthermore, MeCN as a solvent performed poorly unless NaCl was added (Table 5, entries 4 and 5). EtOAc showed the best performance, and the presence of NaCl had no effect (Table 5, entries 6 and 7). Other non-alcohol solvents like THF, DMSO and cyrene were also tested, but resulted in low yields (Table 5, entries 8–10).

After identifying the optimal solvent, we focused on determining the ideal catalyst loading, particularly the optimal TEMPO/Fe(NO<sub>3</sub>)<sub>3</sub> ratio. Interestingly, previous research<sup>27</sup> indicated that a 1 : 1 ratio of TEMPO to Fe(NO<sub>3</sub>)<sub>3</sub> was not always optimal, with a 5 mol%/2.5 mol% ratio yielding better results than a 5 mol%/5 mol% ratio in acetonitrile. To address this issue, a full catalyst ratio screening was conducted in EtOAc. Starting with a 5 mol%/5 mol% ratio, we observed that increasing the loading to either 5 mol%/10 mol% or 10 mol%/5 mol% did not lead to a significant increase in yield.

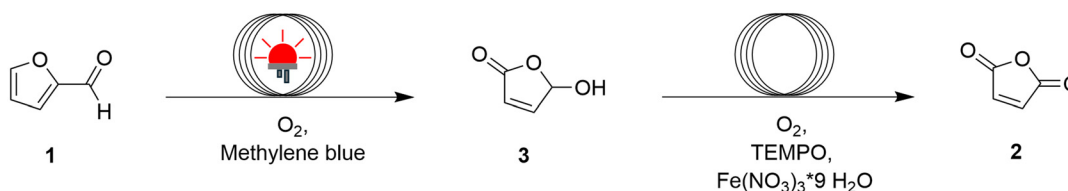


Fig. 5 This work: a two-step continuous flow process to synthesize MA **2**.

Table 4 Reaction optimization of the singlet oxygen oxidation of FUR **1** towards HFO **3**

Entry	Pump flow rate (ml min <sup>-1</sup> )	O <sub>2</sub> flow rate (ml <sub>N</sub> min <sup>-1</sup> )	Residence time (min)	Conv. <b>1</b> <sup>a</sup> (%)	Yield <b>3</b> <sup>a</sup> (%)
1	1.5	20	10	87	79
2	1	13.33	15	95	94
3	0.75	10	20	100	100

<sup>a</sup> Conversion and yield determined *via* quantitative HPLC analysis.



**Table 5** Solvent screening for the aerobic oxidation of HFO **3** to MA **2** in batch

Entry	Solvent	NaCl (mol%)	Reaction time (h)	Yield <b>2</b> <sup>a</sup> (%)
1	MeOH	—	2 4,5	0 0
2	EtOAc/MeOH (99/1)	—	2 4,5	4 8
3	H <sub>2</sub> O	—	2 4,5	0 0
4	MeCN	—	2 4,5	14 23
5	MeCN	25	2 4,5	45 62
6	EtOAc	—	2 4,5	60 80
7	EtOAc	25	2 4,5	63 78
8	THF	—	2 4,5	10 21
9	DMSO	—	2 4,5	0 0
10	Cyrene	—	2 4,5	0 0

<sup>a</sup>Based on <sup>1</sup>H-NMR analysis, no by-products were detected, and the yield of MA was found to be equal to the conversion of furfural when verified using an internal standard. Thus, the yield was estimated using the following formula: yield = MA/(FUR + MA) via <sup>1</sup>H-NMR analysis.

Therefore, we concluded that in EtOAc, a catalyst ratio of 1 : 1 is optimal and a 7.5 mol%/7.5 mol% loading was used in the following experiments (Fig. S15, ESI†).

In the next step of the optimization process, temperature variation was evaluated. It was hypothesized that, if the reaction is O<sub>2</sub> limited, lowering the temperature might positively affect the oxidation reaction due to an increased oxygen solubility. However, the reaction was significantly attenuated at 0 °C. In TEMPO-mediated oxidations of primary alcohols to aliphatic aldehydes, careful temperature control is recommended due to the potential risk of overoxidation to carboxylic acids at higher temperatures.<sup>45</sup> However, the butanolide system **3** displays little risk of overoxidation in its ring-closed form. As such, we found that increasing the temperature significantly accelerated the reaction rate, resulting in a 90% yield in just 30 minutes with little to no side product formation (Table 6). This significant decrease in reaction time paves the way for implementing a continuous flow process.

#### Continuous flow optimization of TEMPO-mediated oxidation of HFO to MA

Working with oxygen at higher temperatures presents several challenges. Since oxygen solubility decreases with increasing

**Table 6** Temperature screening for the aerobic oxidation of HFO **3** to MA **2** in batch

Entry	Temperature (°C)	Reaction time (h)	Yield <b>2</b> <sup>a</sup> (%)
1	0	2 4,5	14 15
2	25	2 4,5	73 97
3	50	0,5 1	90 100

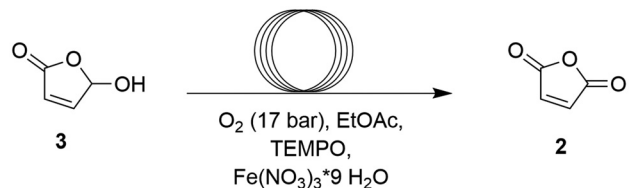
<sup>a</sup>Based on <sup>1</sup>H-NMR analysis, no by-products were detected, and the yield of MA was found to be equal to the conversion of furfural when verified using an internal standard. Thus, the yield was estimated using the following formula: yield = MA/(FUR + MA) via <sup>1</sup>H-NMR analysis.

temperature, maintaining a constant supply of oxygen in a batch setup can be difficult due to the limited headspace and the limited interphase surface area. In contrast, a continuous flow setup offers a more elegant solution. By using a reaction mixture-oxygen Taylor flow, it ensures a consistent supply of oxygen which is readily taken up by the mixture due to the high interphase surface area while also allowing for safe operation at higher pressures and temperatures. In a continuous flow system, temperatures can be substantially increased compared to batch processes because the back pressure exerted on the reaction mixture raises the solvent's boiling point, allowing it to remain in a liquid state even above its atmospheric boiling temperature. It was observed that at 70 °C, a 98% conversion could be achieved in just 15 minutes, while at 50 °C it takes 30 minutes to achieve 98% conversion. Increasing the temperature to 100 °C further accelerated the reaction rate, but this temperature could not be utilized due to reproducibility issues (Table 7, entries 1–3). The final step was to increase the product concentration to enhance productivity. It was observed that higher concentrations led to improved yields within the same reaction time (Table 7, entry 4). At a concentration of 0.2 M, it was observed that the catalyst loading could be lowered to 2 mol% while still maintaining near-quantitative yield after 15 minutes (Table 7, entries 5–7). However, further reducing the catalyst loading resulted in incomplete conversion (Table 7, entry 7).

#### Continuous flow oxidation of FUR to MA without intermediate purification

A final step to minimize waste production is to directly link the two reaction steps without performing intermediate purification. Since the first oxidation step from FUR to HFO does not produce any side products, the only potential impurity in the second oxidation is methylene blue, which should remain



**Table 7** Continuous flow optimization of the aerobic oxidation of HFO 3 to MA 2


Entry	Conc. (M)	Cat. loading (mol%)	Reaction mixture flow (ml min <sup>-1</sup> )	Oxygen flow (ml <sub>N</sub> min <sup>-1</sup> )	Temp. (°C)	RT (min)	Conversion 3 <sup>a</sup> (yield 2) (%)
1	0.05	TEMPO (7.5) Fe(NO <sub>3</sub> ) <sub>3</sub> (7.5)	1.4	16	50	5	58 (58)
			0.7	8		10	68 (68)
			0.23	2.66		30	98 (96)
2	0.05	TEMPO (7.5) Fe(NO <sub>3</sub> ) <sub>3</sub> (7.5)	1.4	16	70	5	69 (69)
			0.7	8		10	86 (84)
			0.47	5.33		15	98 (98)
3	0.05	TEMPO (7.5) Fe(NO <sub>3</sub> ) <sub>3</sub> (7.5)	0.7	8	100	10	92 (92)
4	0.1	TEMPO (7.5) Fe(NO <sub>3</sub> ) <sub>3</sub> (7.5)	1.4	16	70	5	99 (98)
			0.7	8		10	100 (100)
5	0.2	TEMPO (3.75) Fe(NO <sub>3</sub> ) <sub>3</sub> (3.75)	2.8	32	70	2.5	72 (72)
			1.4	16		5	98 (97)
6	0.2	TEMPO (2) Fe(NO <sub>3</sub> ) <sub>3</sub> (2)	1.4	16	70	5	57 (57)
			0.47	5.33		15	97 (97)
			0.23	2.66		30	100 (99)
7	0.2	TEMPO (1.5) Fe(NO <sub>3</sub> ) <sub>3</sub> (1.5)	0.23	2.66	70	30	93 (92)

<sup>a</sup> Yield and conversion are determined *via* <sup>1</sup>H-NMR analysis with mesitylene as internal standard.

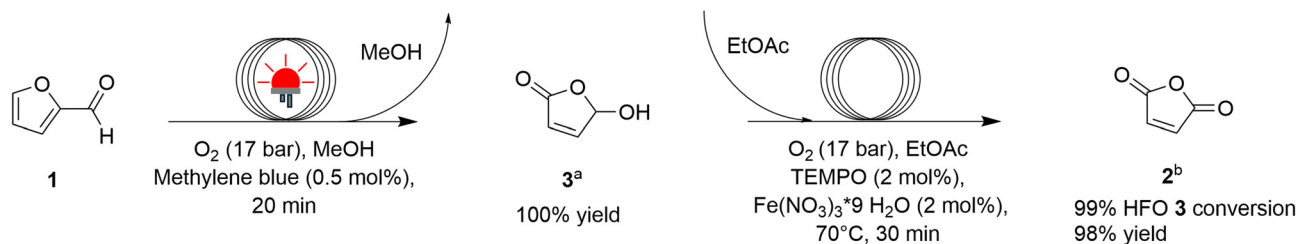


**Fig. 6** Continuous flow oxidation of FUR 1 to MA 2 without intermediate purification. <sup>a</sup> Yield is determined *via* quantitative HPLC analysis after first reaction step. <sup>b</sup> Yield and conversion are determined *via* <sup>1</sup>H-NMR analysis with mesitylene as internal standard which was added after the first reaction step.

inactive if shielded from light. However, it is crucial to completely evaporate MeOH before dissolving the reaction mixture in EtOAc for the second reaction step, as even small amounts of MeOH were found to completely halt the reaction (Table 5, entry 2). It was observed that the reaction with the unpurified intermediate still resulted in a high yield of 98% maleic anhydride (Fig. 6).

## Conclusions

This study provides valuable insights into the O<sub>2</sub><sup>1</sup> oxidation of furfural, underscoring the critical role of solvent choice in product selectivity and offering a detailed overview of the product range. It concludes that a one-step singlet oxygen oxidation of furfural to maleic anhydride is inefficient due to low

selectivity, but in the process, valuable insights in the potential reaction mechanism of O<sub>2</sub><sup>1</sup> furfural oxidation were found. Instead, an existing two-step pathway has been optimized to create a highly selective, productive, and scalable route towards maleic anhydride in a green manner. It should be noted that the solvents used in the pathway, are both classified as 'recommended' according to the CHEM21 selection guide of classical- and less classical-solvents.<sup>46</sup> In the process, both reaction steps utilize catalysts, with oxygen being the only reagent used in stoichiometric amounts. Unlike previous methods, this approach avoids excessive heating, as the first step is conducted at room temperature and the second step at just 70 °C. This method minimizes waste by eliminating the need for intermediate purification between the reaction steps. A final enhancement achieved by utilizing continuous flow is the improved safety when operating under higher pressures.





## Data availability

The data supporting this article have been included as part of the ESI.†

## Conflicts of interest

There are no conflicts to declare.

## Acknowledgements

Jonas Mortier gratefully acknowledges financial support for this publication by the Ghent University Special Research Fund; grant nr. BOF/STA/202102/003.

## References

- 1 E. Gawel, N. Pannicke and N. Hagemann, *Sustainability*, 2019, **11**, 3005.
- 2 T. L. Chen, H. Kim, S. Y. Pan, P. C. Tseng, Y. P. Lin and P. C. Chiang, *Sci. Total Environ.*, 2020, **716**, 136998.
- 3 R. Mariscal, P. Maireles-Torres, M. Ojeda, I. Sádaba and M. L. López Granados, *Energy Environ. Sci.*, 2016, **9**, 1144–1189.
- 4 A. S. Mamman, J. M. Lee, Y. C. Kim, I. T. Hwang, N. J. Park, Y. K. Hwang, J. S. Chang and J. S. Hwang, *Biofuels, Bioprod. Biorefin.*, 2008, **2**, 438–454.
- 5 K. Lohbeck, H. Haferkorn, W. Fuhrmann and N. Fedtke, in *Ullmann's Encyclopedia of Industrial Chemistry*, Wiley, 2000.
- 6 E.-R. Kenawy and M. A. Sakran, *J. Appl. Polym. Sci.*, 2001, **80**, 415–421.
- 7 G. Cent, F. Trifirb, J. R. Ebner' and V. M. Franchetti, *Chem. Rev.*, 1988, **88**, 55–80.
- 8 B. K. Hodnett, *Catal. Rev.*, 1985, **27**, 373–424.
- 9 N. F. Dummer, J. K. Bartley and G. J. Hutchings, *Adv. Catal.*, 2011, **54**, 189–247.
- 10 N. Ballarini, F. Cavani, C. Cortelli, S. Ligi, F. Pierelli, F. Trifirò, C. Fumagalli, G. Mazzoni and T. Monti, *Top. Catal.*, 2006, **38**, 147–156.
- 11 P. Santander, L. Bravo, G. Pecchi and A. Karelavic, *Appl. Catal., A*, 2020, **595**, 117513.
- 12 X. Li, J. Ko and Y. Zhang, *ChemSusChem*, 2018, **11**, 612–618.
- 13 N. Alonso-Fagúndez, M. Ojeda, R. Mariscal, J. L. G. Fierro and M. López Granados, *J. Catal.*, 2017, **348**, 265–275.
- 14 N. Alonso-Fagúndez, M. López Granados, R. Mariscal and M. Ojeda, *ChemSusChem*, 2012, **5**, 1984–1990.
- 15 X. Li, B. Ho and Y. Zhang, *Green Chem.*, 2016, **18**, 2976–2980.
- 16 G. Lv, C. Chen, B. Lu, J. Li, Y. Yang, C. Chen, T. Deng, Y. Zhu and X. Hou, *RSC Adv.*, 2016, **6**, 101277–101282.
- 17 J. Lan, Z. Chen, J. Lin and G. Yin, *Green Chem.*, 2014, **16**, 4351–4358.
- 18 Md. M. Baag, A. Kar and N. P. Argade, *Tetrahedron*, 2003, **59**, 6489–6492.
- 19 H. Tateno, Y. Miseki, H. Kusama, S.-Y. Chen, T. Mochizuki and K. Sayama, *ACS Sustainable Chem. Eng.*, 2021, **9**, 6886–6893.
- 20 M. Hofmann, M. Garrido, M. Machado, J. R. Correia and J. C. Bordado, *J. Appl. Polym. Sci.*, 2022, **139**, e53029.
- 21 Y. Yu, H. Xiong, J. Xiao, X. Qian, X. Leng, Z. Wei and Y. Li, *ACS Sustainable Chem. Eng.*, 2019, **7**, 6859–6869.
- 22 D. Sun, F. Sato, Y. Yamada and S. Sato, *Bull. Chem. Soc. Jpn.*, 2013, **86**, 276–282.
- 23 J. Agarwal, R. Rani and R. Peddinti, *Synlett*, 2017, 1336–1340.
- 24 D. A. Kornilov, I. F. Dinikaev and V. D. Kiselev, *High Pressure Res.*, 2019, **39**, 640–654.
- 25 J. D. Williams, M. Nakano, R. Gérardy, J. A. Rincón, Ó. de Frutos, C. Mateos, J.-C. M. Monbaliu and C. O. Kappe, *Org. Process Res. Dev.*, 2019, **23**, 78–87.
- 26 E. Torres, E. Gorrea, K. K. Burusco, E. Da Silva, P. Nolis, F. Rúa, S. Boussert, I. Díez-Pérez, S. Dannenberg, S. Izquierdo, E. Giralt, C. Jaime, V. Branchadell and R. M. Ortuño, *Org. Biomol. Chem.*, 2010, **8**, 564–575.
- 27 J. G. H. Hermens, A. Jensma and B. L. Feringa, *Angew. Chem., – Int. Ed.*, 2022, **61**, e202112618.
- 28 C. Robert, F. de Montigny and C. M. Thomas, *ACS Catal.*, 2014, **4**, 3586–3589.
- 29 W. Jia, Z. Si, Y. Feng, X. Zhang, X. Zhao, Y. Sun, X. Tang, X. Zeng and L. Lin, *ACS Sustainable Chem. Eng.*, 2020, **8**, 7901–7908.
- 30 W. Jia, Y. Sun, M. Zuo, Y. Feng, X. Tang, X. Zeng and L. Lin, *ChemSusChem*, 2020, **13**, 640–646.
- 31 X. Li, B. Ho, D. S. W. Lim and Y. Zhang, *Green Chem.*, 2017, **19**, 914–918.
- 32 P. Ren, Y. Zhou, K. Su, L. Sun, N. Luo and F. Wang, *Chem. – Asian J.*, 2023, **18**, e202300732.
- 33 D. K. Chauhan, V. R. Battula, A. Giri, A. Patra and K. Kailasam, *Catal. Sci. Technol.*, 2022, **12**, 144–153.
- 34 J. de Jong and B. Feringa, *Tetrahedron: Asymmetry*, 1991, **2**, 1247–1262.
- 35 X. Zhang, H. H. Huang and Q. H. Chen, *J. Asian Nat. Prod. Res.*, 2005, **7**, 711–721.
- 36 M. D. Edwards, M. T. Pratley, C. M. Gordon, R. I. Teixeira, H. Ali, I. Mahmood, R. Lester, A. Love, J. G. H. Hermens, T. Freese, B. L. Feringa, M. Poliakov and M. W. George, *Org. Process Res. Dev.*, 2024, **28**, 1917–1928.
- 37 J. G. H. Hermens, M. L. Lepage, A. Kloekhorst, E. Keller, R. Bloem, M. Meijer and B. L. Feringa, *React. Chem. Eng.*, 2022, **7**, 2280–2284.
- 38 S. Thiagarajan, D. Franciolus, R. J. M. Bisselink, T. A. Ewing, C. G. Boeriu and J. Van Haveren, *ACS Sustainable Chem. Eng.*, 2020, **8**, 10626–10632.
- 39 A. M. S. Pembere, H. Louis and H. Wu, *J. Mol. Model.*, 2023, **29**, 359.
- 40 N. Alonso-Fagúndez, I. Agirrezabal-Telleria, P. L. Arias, J. L. G. Fierro, R. Mariscal and M. López Granados, *RSC Adv.*, 2014, **4**, 54960–54972.
- 41 M. R. Ebrahimian, M. Tavakolian and M. Hosseini-Sarvari, *J. Environ. Chem. Eng.*, 2023, **11**, 109347.



- 42 J. G. H. Hermens, T. Freese, G. Alachouzos, M. L. Lepage, K. J. van den Berg, N. Elders and B. L. Feringa, *Green Chem.*, 2022, **24**, 9772–9780.
- 43 S. Ma, J. Liu, S. Li, B. Chen, J. Cheng, J. Kuang, Y. Liu, B. Wan, Y. Wang, J. Ye, Q. Yu, W. Yuan and S. Yu, *Adv. Synth. Catal.*, 2011, **353**, 1005–1017.
- 44 D. E. Fitzpatrick and S. V. Ley, *Tetrahedron*, 2018, **74**, 3087–3100.
- 45 B. L. Ryland and S. S. Stahl, *Angew. Chem., – Int. Ed.*, 2014, **53**, 8824–8838.
- 46 D. Prat, A. Wells, J. Hayler, H. Sneddon, C. R. McElroy, S. Abou-Shehadeh and P. J. Dunn, *Green Chem.*, 2015, **18**, 288–296.

